Materials Advances

ROYAL SOCIETY OF CHEMISTRY

PAPER

View Article Online
View Journal | View Issue

Cite this: *Mater. Adv.*, 2025, 6, 9011

Scaffold-free biofabrication of tissue engineered trachea by cartilage microtissue assembly

Long Wang,†[ab] Weikang Lin,†[ab] Lei Zhang,[ab] Yunlang She,[ab] Weiyan Sun,[ab] Hai Tang,[ab] Chao Lin *[c] and Chang Chen *[ab]

Received 23rd February 2025,
Accepted 8th October 2025

DOI: 10.1039/d5ma00172b

rsc.li/materials-advances

Currently, there is no ideal scaffold for tissue engineering of the trachea to treat long-segmental tracheal defects in clinical practice. Given the desirable properties of cartilage regeneration and its self-fusion nature, chondrocyte spheroids serve as promising building blocks for robust mechanical cartilaginous tissue for engineering trachea construction. Herein, a bottom-up self-assembly approach based on chondrocyte spheroids was developed to reconstruct resilient scaffold-free trachea. Employing custom-designed molds for spheroid assembly, we identified an optimal seeding density of 2000 cells per microwell that consistently produced spheroids of approximately 163.7 ± 9.0 μm, which yielded spheroids with superior cartilage matrix secretion and significantly upregulated the expression of SOX9, ACAN and COL2A1. We fabricated scaffold-free tracheas with robust mechanical integrity with a Young's modulus of 3.5 ± 0.3 MPa. Safranin O, Alcian Blue, and collagen II immunohistochemical staining analyses of the scaffold-free tracheas indicated consecutive cellular and accumulated matrix distribution inside the microtissues. After maturation *in vivo* for 4 weeks, the primitive spheroids had completely fused and formed mature cartilage tissue, and the fibrous arrangement of the cartilage was similar to that of native cartilage. Immunohistochemical staining for CD31 confirmed the presence of extensive vascularization within the engineered tracheal constructs, indicating successful functional integration with the host tissue. Overall, this study highlights a bottom-up self-assembly strategy using spheroids, making it possible to construct macroscopic, large-scale tracheas through a standardized, repeatable, high-flux approach.

1. Introduction

Tracheal defects normally result from trauma, tumors, and stenosis in clinical settings. Short-segment defects can be treated by end-to-end anastomosis.[1] However, in the context of long tracheal defects, end-to-end anastomosis is associated with excessive tension, potentially leading to fatal complications.[2,3] In addition, allogeneic tracheal transplantation requires repeated administration of immunosuppressive drugs, which limits its clinical applications.[4] Thus, the reconstruction of long-segmental tracheal defects remains a significant challenge.

In recent years, numerous studies have explored scaffold-based tracheal substitutes, including decellularized matrices, electrospinning, casting, and 3D printing.[3–9] However, scaffold-based constructs often suffer from mechanical mismatch, poor vascularization, and chronic inflammation, leading to graft failure.[1,3,7,8] Scaffold-free approaches, such as cell sheets or cellular gels, improve biocompatibility but remain fragile, with limited thickness and inadequate strength for long tubular reconstruction. In this context, spheroid-based assembly offers distinct advantages: spheroids provide a high-density extracellular matrix and enhanced fusion capacity, mimic developmental condensation processes, and can be modularly assembled in molds to recreate the asymmetric cartilage, membrane anatomy of a native trachea.[10–13] Furthermore, spheroids can integrate endothelial or stromal cells, facilitating prevascularization and improved matrix maturation after implantation. These features address both structural and vascularization challenges, positioning spheroid-based biofabrication as a uniquely suited strategy for functional tracheal regeneration.

The availability of a tubular-like scaffold is limited due to complex synthesis, fabrication and structural design. Alternatively, scaffold-free tissue engineering using 3D-cultured cells (spheroids) facilitates the reconstruction of macroscopic tissues,[14–16] due to high cell density and the generation of an

[a] *Department of Thoracic Surgery, Shanghai Pulmonary Hospital, School of Medicine, Tongji University, Shanghai 200433, China. E-mail: chenthoracic@163.com*
[b] *Shanghai Engineering Research Center of Lung Transplantation, Shanghai 200433, China*
[c] *The Institute for Biomedical Engineering and Nanoscience, Tongji University School of Medicine, Shanghai 200092, China. E-mail: chaolin@tongji.edu.cn*
† These authors contributed equally to this work.

extracellular matrix (ECM). Chondrocytes are central to hyaline cartilage formation, which is defined by an abundant extracellular matrix rich in type II collagen and glycosaminoglycans (GAGs). In 3D spheroid culture, chondrocytes spontaneously aggregate, fuse, and upregulate cartilage-specific genes, leading to enhanced secretion of these matrix components and maturation into tissue-like constructs.[11,17] This ability relies on enhanced three-dimensional cell–cell interactions and intensive cell–matrix interactions. These features provide measurable indicators of success in scaffold-free cartilage engineering and form the biological basis for applying spheroid-based assembly to tracheal regeneration.

As a kind of microtissue, chondrocyte spheroids may serve as "building blocks" for tracheal tissue engineering due to their microscopic dimensions and abundant ECM deposition. Recent innovations in spheroid biofabrication have enabled the precise spatial organization of chondrogenic units, producing cartilage constructs with native-like zonal architecture. Co-culture and microfluidic strategies have yielded vascularized spheroids, improving integration potential in tubular constructs. Porous microscaffold-templated spheroids further enhance fusion efficiency, accelerating the maturation of engineered cartilage and tracheal tissues. Beyond the trachea, scaffold-free chondrocyte spheroid strategies may be adapted for other cartilage-based tissues that rely on type II collagen and glycosaminoglycan, including auricular and intervertebral disc cartilage.[10,14,16–19] This generalizability underscores the broader regenerative potential of spheroid-driven tissue assembly.

Taken together, these considerations motivated us to explore a scaffold-free strategy for engineering tracheal cartilage. We hypothesized that a scaffold-free tracheal construct composed of modular chondrocyte spheroids would not only display cartilage-like extracellular matrix characteristics but also support structural maturation following implantation. To test this, we optimized spheroid parameters to enhance matrix deposition, employed agarose molds to guide trachea shaping, and evaluated the functional maturation of the engineered trachea after implantation. The aim of this study was therefore to develop and validate a systematized approach for spheroid assembly into a scaffold-free trachea construct, with emphasis on its structural organization, functional stability, and translational potential (Fig. 1).

2. Results

2.1. Aggregation of chondrocyte spheroids and optimization of culture conditions

Primary chondrocytes were seeded into microwells in different quantities (1k, 2k, 4k, 8k and 16k). The chondrocytes aggregated into spheroidal microtissues 24 h after seeding (Fig. 2A and Fig. S1E–I). The diameters of the spheroids in the groups listed above were 132.99 ± 7.86 μm, 163.69 ± 9.01 μm, 218.91 ± 19.88 μm, 283.88 ± 20.66 μm, and 354.50 ± 17.47 μm, respectively (Fig. S1J). Furthermore, the diameters of the spheroids in all groups had a normal distribution (Fig. S1K). The circularity values of the spheroids were 0.92 ± 0.04, 0.87 ± 0.07, 0.91 ± 0.04, 0.82 ± 0.13, and 0.95 ± 0.03 in the five groups, respectively (Fig. 2E). Regression analysis revealed that the diameter, 24 h after seeding, exhibited a linear correlation with the cubic root of the number of cells. The regression function of cell number (x, cells) and diameter (d, μm) was $d = 15.020\sqrt[3]{x} - 19.572$

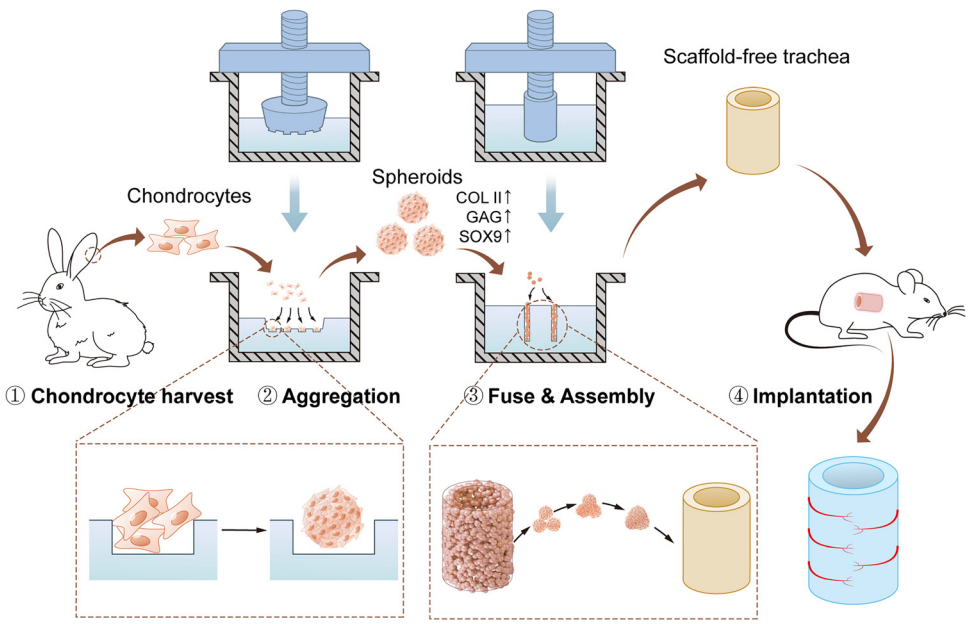

Fig. 1 Scheme of the study design. Primary chondrocytes were harvested from rabbit ear cartilage. Passage 3 chondrocytes were seeded into low-adhesion microwells to aggregate the spheroids. Then, spheroids were self-assembled into ring-like units resembling a scaffold-free trachea mold. Afterwards, the scaffold-free trachea was subcutaneously implanted into the back of BALB/c nude mice, and its chondrogenic and mechanical properties were evaluated.

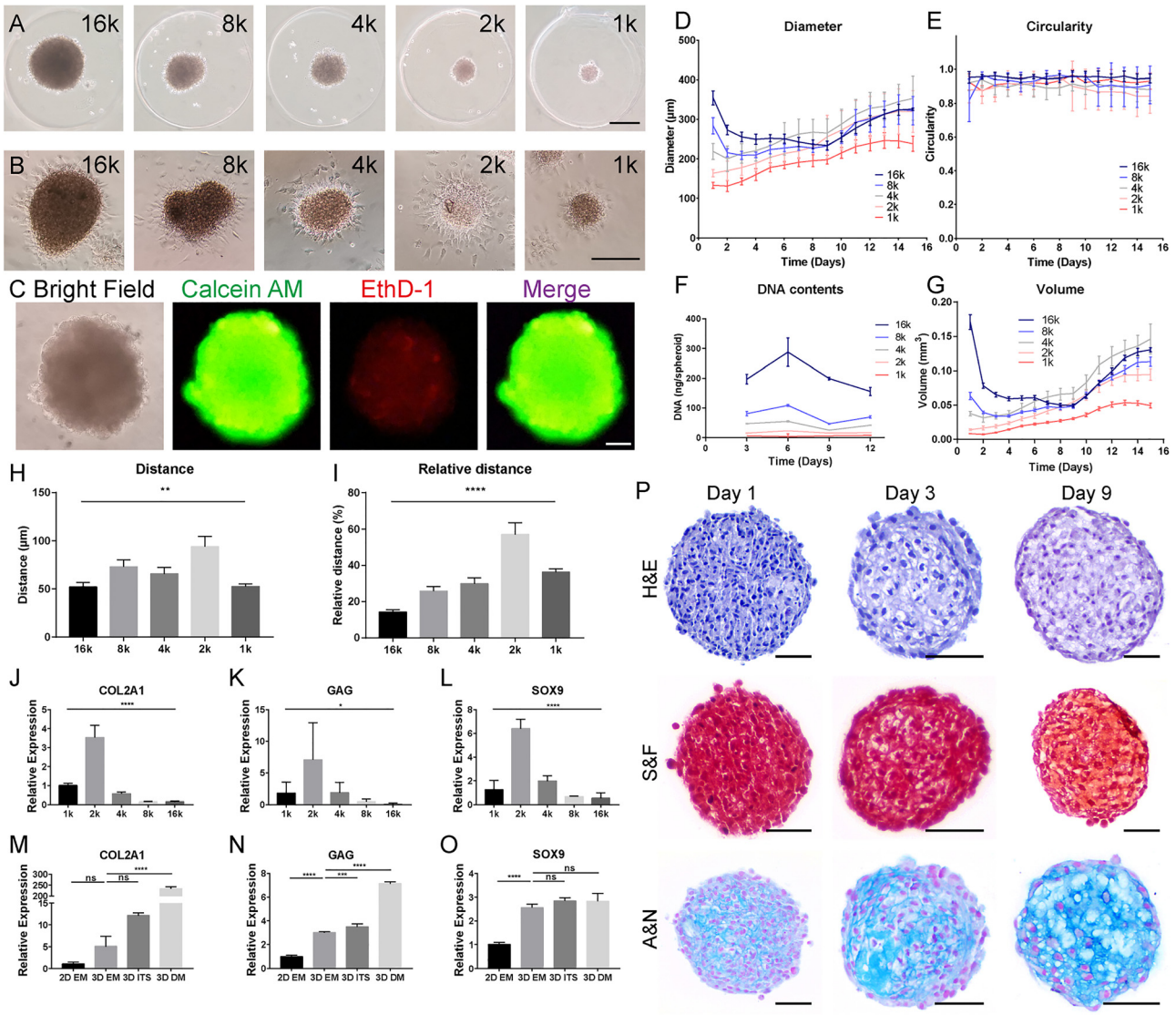

Fig. 2 Characteristics of the spheroids. (A) The 1k, 2k, 4k, 8k and 16k chondrocyte spheroids under the microscope. (B) Brightfield images and live/dead staining of spheroids. (C) Chondrocyte spheroids formed from different numbers of chondrocytes were transferred onto non-low-attachment dishes for 24 h. (D) Diameters of chondrocyte spheroids formed from different numbers of chondrocytes. (E) Circularity of chondrocyte spheroids formed from different numbers of chondrocytes. (F) Average DNA content for spheroids formed from different numbers of chondrocytes. (G) Volume of spheroids formed from different numbers of chondrocytes. (H) and (I) Migration distances and relative migration distances of the spheroids. (J)–(L) Relative mRNA expression of COL2A1, GAG, and SOX9 in spheroids self-assembled from different numbers of chondrocytes. (M)–(O) Relative mRNA expression of COL2A1, GAG, and SOX9 in spheroids cultured in different culture media and using different culture methods. (P) Histological examination of the microtissues after 1, 7, and 15 days of culture and staining with hematoxylin and eosin, Safranin O/Fast Green and Alcian Blue/Nuclear Fast Red. EM, expansion medium; DM, differentiation medium; ITS, insulin–transferrin–selenium medium.

(Fig. S1J). Live/dead staining showed that nearly all cells in the spheroids were stained green, with only a few cells stained red (Fig. 2B). The spheroids were then transferred onto non-low-attachment dishes for 24 h in expansion medium. All spheroids were seen to undergo cell migration from the edges (Fig. 2C). Spheroids in different groups were cultured for 15 d, and major and minor diameters were recorded daily (Fig. 2D). During 15 d of culture, the diameters of the spheroids first decreased and then increased with time, while the circularity remained greater than 0.90 (Fig. 2E). DNA from the spheroids was extracted from cultures with different cell numbers and culture times. The DNA content in the 1k-, 2k-, 4k-, 8k-, and 16k-cell groups remained stable (Fig. 2F). The volume of each spheroid was calculated from $V = 4\pi ab^2/3$ (V, volume; a, major diameter; b, minor diameter), and the volume of the spheroids in each group tended to first decrease and then increase (Fig. 2G). This indicated that the volume increase was due to ECM accumulation rather than chondrocyte proliferation.

Fig. 2C shows the cell migration of each group. The distance of migration was measured for each group. As shown in Fig. 2H, the cells in the 2k-cell group migrated the furthest among the five groups, and the difference was significant ($P = 0.0037$). The relative distances (distance/diameter) showed

the same result ($P < 0.0001$) (Fig. 2I). Moreover, cartilage-related gene expression in spheroids with different cell numbers was compared. The PCR results showed that the 2k-cell group expressed higher levels of COL2A1 ($P < 0.0001$), GAG ($P = 0.012$), and SOX9 ($P < 0.0001$) than the other groups (Fig. 2J–L). We compared cartilage-related gene expression between cells in spheroids and conventional chondrocytes in dishes. In the spheroid group, the cells expressed higher levels of COL2A1 ($P = 0.3756$), GAG ($P < 0.0001$), and SOX9 ($P < 0.0001$) than conventional chondrocytes. Then, spheroids were cultured in differentiation medium (DM) to examine their behavior under optimized culture conditions. Insulin–transferrin–selenium (ITS) medium induced upregulation of COL2A1 ($P = 0.0574$) expression, and DM induced upregulation of COL2A1 ($P < 0.0001$) and GAG ($P < 0.0001$) expression. All three types of medium induced upregulation of COL2A1 ($P < 0.0001$), GAG ($P < 0.0001$), and SOX9 ($P < 0.0001$) expression (Fig. 2M–O).

Histological examination of the spheroids revealed their development during culture (Fig. 2P). On day 1, the chondrocytes aggregated together, with no sign of cell arrangement. As time passed, the cells in the outer part of each spheroid grew longer and thinner, becoming a membrane wrapping the spheroid. The interstitial spaces grew larger, with light blue staining, and cartilage lacunae formed at the center of the tissue. Safranin O/Fast Green staining and Alcian Blue/Nuclear Fast Red staining showed the matrix accumulation process inside the spheroids.

2.2. Fusion behavior of chondrocyte spheroids

Two chondrocyte spheroids were placed into the same microwell to study the fusion process. To quantitatively characterize the spheroid fusion process, we monitored spheroid doublets in DMEM (Dulbecco's modified Eagle medium) supplemented with 10% fetal bovine serum (FBS) and 1% penicillin–streptomycin (PS) under 37 °C, 5% CO_2. Contact between the two spheroids was observed on day 3, and the cells underwent a fusion process. The two spheroids came into contact with each other on day 8 (Fig. 3A). The interface expanded rapidly, and the two spheroids approached each other. The doublet length decreased, the contact length increased rapidly, and the intersphere angle ultimately changed from acute to obtuse. The fusion process is summarized in Fig. 3B. Doublet length, doublet width, intersphere angle and contact length were measured daily, and the results are shown in Fig. 3C and D. Based on these parameters, we determined that stable fusion was typically achieved within 5–7 days. The intersphere angles increased rapidly and then tended to remain stable at 180°. Doublet length and width decreased slightly and then increased slowly. The contact length increased rapidly and then continued to increase slowly.

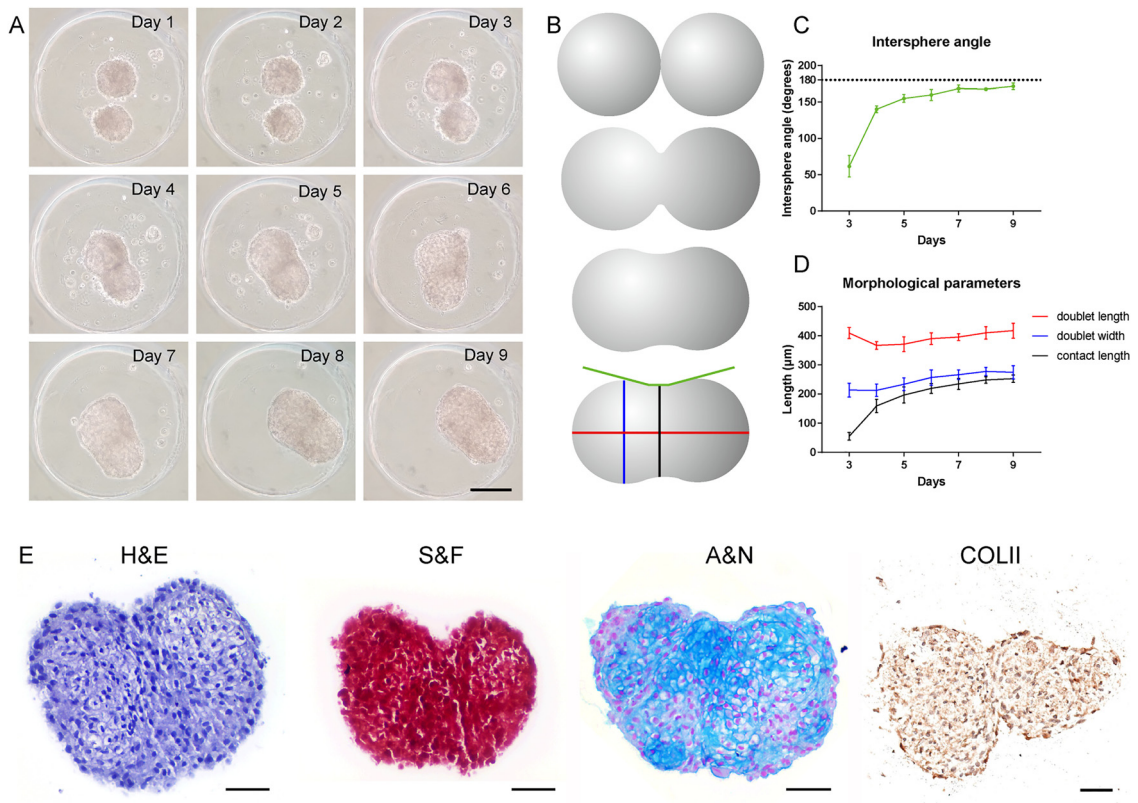

Fig. 3 Fusion properties of the microtissues. (A) Daily microscopic changes in two microtissues placed in a microwell together. (B) Schematic diagram of doublet length, doublet width, intersphere angle, and contact length measurements. (C) and (D) Quantification of the intersphere angle and morphological changes of the doublets. (E) Hematoxylin and eosin, Safranin O/Fast Green, Alcian Blue/Nuclear Fast Red, and collagen II immunohistochemical staining of doublets. COL II, collagen II.

The histological results showed that the spheroids fused into a microtissue, and the contact region of the doublets fused tightly, with no space remaining (Fig. 3E). The chondrocytes came into contact with each other, and matrix accumulation was then observed. Safranin O/Fast Green staining and Alcian Blue/Nuclear Fast Red staining showed the connection between the two spheroids. Immunohistochemistry for COLII showed widespread extracellular type II collagen accumulation.

2.3. Scaffold-free biofabrication of large-scale engineered tracheas

Scaffold-free tracheas were biofabricated with the help of tubular agarose molds (Fig. 4A). Briefly, spheroids were generated and collected, and then the spheroids were injected into tubular molds and accumulated as tubular structures. The spheroids came into contact with each other, and then the fusion process occurred. After self-assembly, a tubular scaffold-free trachea was fabricated (Fig. 4B–D). After 28 days of culture,

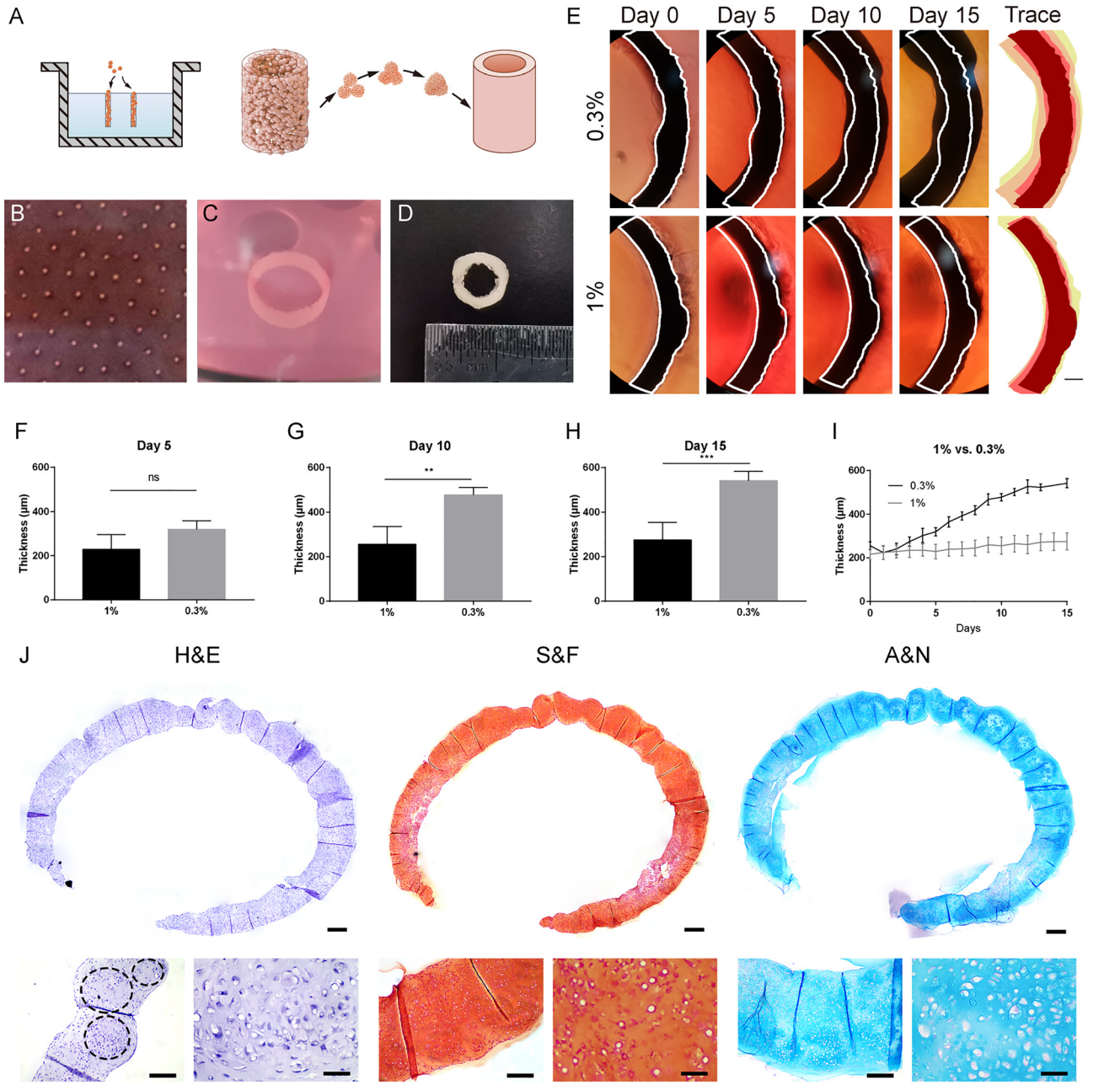

Fig. 4 Biofabrication of scaffold-free tracheas. (A) Schematic diagram of scaffold-free trachea fabrication. (B) Brightfield image of the microtissue. (C) and (D) Macro view of a scaffold-free trachea. (E) Microscopic morphology changes of the scaffold-free tracheal wall in molds with different agarose concentrations. (F)–(I) The wall thickness of scaffold-free tracheas fabricated in 1% and 0.3% agarose molds after different culture times. (J) Hematoxylin and eosin, Safranin O/Fast Green, Alcian Blue/Nuclear Fast Red staining of scaffold-free tracheas *in vitro*.

scaffold-free tracheas were successfully harvested. For tubular construct assembly, approximately 1000 spheroids, derived from $\sim 2 \times 10^6$ chondrocytes, were placed in a tubular structure. The outside diameter was approximately 7.5 mm, and the inside diameter was approximately 5.0 mm, with a wall thickness of approximately 1.2 mm (Fig. S2).

After spheroid seeding, images of the same field of view were captured daily. The results showed that the edges of the tubes became smooth, and spheroidal contours disappeared on day 1 compared with day 0, indicating that the microtissues had fused and self-assembled into a whole tube (Fig. 4E and Fig. S3A). During the 5–7 day incubation period, spheroids fused to form a continuous ring structure, with morphological stability confirmed by daily observation, as documented in Fig. 4E and I. These results confirm the reproducibility and robustness of spheroid fusion in forming scaffold-free engineered tracheal constructs.

Furthermore, the scaffold-free tracheas were divided into two groups according to the agarose concentration of the tubular agarose molds. After 15 days of culture, the walls of the scaffold-free tracheas in both the 0.3% and 1% agarose groups gradually became thicker with the support of tubular agarose molds, as shown in Fig. 4E. However, the walls of the tracheas in the 0.3% agarose group seemed to be thicker than those of the tracheas in the 1% agarose group. By performing ImageJ analysis, we estimated the area of the scaffold-free tracheal wall, and we found that the area of the tracheal walls in the 0.3% agarose group increased by 117.06%, while that of the tracheal walls in the 1% agarose group increased by only 66.44%. We also measured the thickness of the tracheal wall in both groups daily (Fig. 4F–I). The day 5 results did not reveal a significant difference ($P = 0.0577$), but on day 10, the thickness of the tracheal wall differed significantly between the two groups ($P = 0.0021$); this difference persisted until day 15, when the thickness of the tracheal wall reached 275.2 ± 39.29 μm *vs.* 542.4 ± 20.23 μm in the 1% *vs.* 0.3% agarose groups ($P = 0.0009$). Daily changes in wall thickness were recorded, as shown in Fig. 4I and Fig. S3B, C. Compared with the 0.3% agarose mold, the 1% agarose mold was able to confine the microtissues better during self-assembly into scaffold-free tracheas to prevent luminal stenosis.

Fig. 4J shows the histological results for the scaffold-free tracheas. The cross sections of the scaffold-free tracheas were annular with uniform thickness. The whole tissue was continuous, and traces of microtissues were observed. Cells in the microtissues were polygonal, with a surrounding cartilage lacuna. Cell divisions were occasionally observed. Abundant ECM staining (light purple) was widely distributed among the cells. Traces of microtissues were observed, with polygonal chondrocytes and a preliminary cartilage lacuna in the center and spindle-shaped chondrocytes in the surrounding region. The interspheroid region was also a light-purple-stained ECM, although a narrower cell distribution was observed.

Safranin O/Fast Green staining of the scaffold-free tracheas showed that the tissues were all stained red, indicating that the tissue was continuous and that cartilage ECM had accumulated. Alcian Blue/Nuclear Fast Red staining showed that the cells distributed in the cartilage lacuna and beyond the lacuna were stained blue. The matrix in spheroidal traces was darker than that in intraspheroidal traces.

2.4 Implantation and maturation of the scaffold-free tracheas

We next aimed to simulate the *in vivo* environment and facilitate further maturation of the scaffold-free tracheas. Scaffold-free tracheas were subcutaneously implanted into the right side of the back in 4-week-old BALB/c nude mice (Fig. 5A). The tracheas were harvested 28 days after implantation, and then histological examination was performed in comparison with the native rabbit trachea.

Fig. 5B shows the histological results for the native rabbit trachea. Ring-shaped cartilage and a fiber membrane enclosed the tracheal lumen. Chondrocytes in the cartilage formed lacunar structures, while the ECM was widely distributed and arranged perpendicular to the surface. Subsequent Safranin O/Fast Green staining and Alcian Blue/Nuclear Fast Red staining showed that the cartilaginous matrix was surrounded the chondrocytes.

As shown in Fig. 5C, the scaffold-free tracheas had a macroscopic structure similar to that of the native tracheas. Hematoxylin and eosin (H&E) staining showed that the scaffold-free tracheas were wrapped by surrounding connective tissues, and the lumen connective tissues were tightly integrated with the implanted cartilage, indicating the high biocompatibility of the implants. The chondrocytes were polygonal, and nuclear division was occasionally observed. Safranin O/Fast Green staining, Alcian Blue/Nuclear Fast Red staining, and subsequent immunohistochemistry (IHC) staining of collagen II showed massive cartilaginous matrix accumulation inside the tracheas, and abundant lacunar structures were seen, similar to natural cartilage tissues, indicating that the implants were full of mature cartilaginous tissue. Blood vessels with red blood cells in the lumen were observed around cartilaginous tissues, and CD31 IHC staining demonstrated vascular endothelial cell growth. This outcome indicates the excellent biocompatibility of the scaffold-free tracheas, as they integrated with the subcutaneous tissues of the nude mice. Furthermore, the nude mice developed neovascularization to supply nutrients to the scaffold-free tracheas, fostering their further maturation.

2.5. Fibrous arrangement and mechanical strength of the scaffold-free tracheas

Under a polarizing microscope, the cartilaginous tissues stained with Sirius Red (SR) exhibited a vibrant color, indicating abundant ECM within the cartilaginous tissue in the native trachea and the scaffold-free trachea (Fig. 6A). Pseudocolor images showed collagen fiber deposition in the cartilage of the scaffold-free trachea, similar to that observed in native tracheal cartilage. The orientation of the collagen fibers was parallel to the surface and reticulated in the deep zones (Fig. 6B).

Then, we cut and expanded the walls of the scaffold-free tracheas to test the mechanical strength of the cartilage tissue. The results showed that the scaffold-free tracheas demonstrated

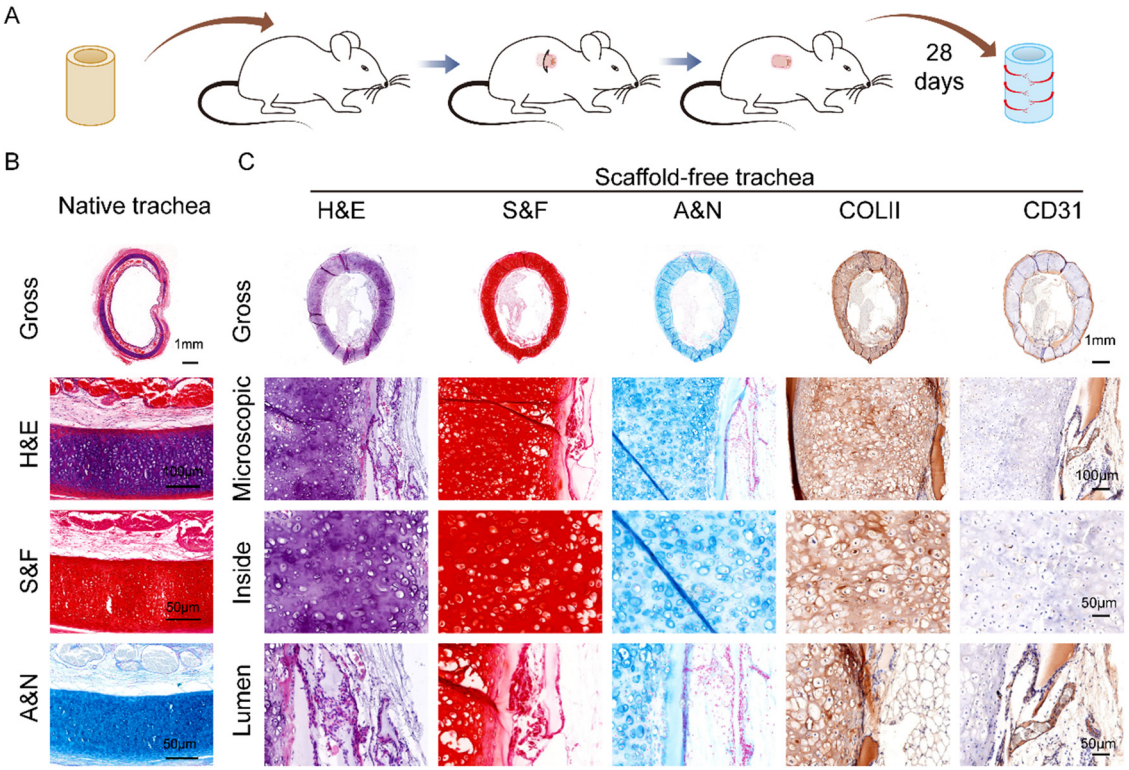

Fig. 5 *In vivo* examination of scaffold-free tracheas. (A) Schematic of scaffold-free trachea transplantation *in vivo*. (B) Histological examination of native tracheas. (C) Histological examination of scaffold-free tracheas *in vivo*. H&E, hematoxylin and eosin staining; S&F, Safranin O/Fast Green staining; A&N, Alcian Blue/Nuclear Fast Red staining; COLII, collagen II immunohistochemical staining.

similar modulus values to the native tracheas but significantly higher modulus values than the *in vitro* tracheas under 50% compression (Fig. 6C). Compared to the native tracheas, the scaffold-free tracheas implanted *in vivo* exhibited a slightly lower maximum stress (Fig. 6D). The Young's modulus of the scaffold-free trachea implanted *in vivo* is slightly lower than that of the native trachea, but significantly higher than that of the scaffold-free trachea implanted *in vitro* (Fig. 6E). This trachea exhibits a strength comparable to that of the native trachea, ensuring resilience under most physiological *in vivo* conditions, including neck movements and the dynamic contraction and relaxation of the trachea.

At half maximum stress, the compression values of the scaffold-free tracheas *in vivo* were similar to those of the native tracheas (Fig. 6F). The finding indicates that the scaffold-free tracheas can withstand similar mechanical conditions to the native tracheas without compromising their structural integrity. Hence, the developed scaffold-free tracheas have great potential as substitutes for long-segmental tracheal grafts.

3. Discussion

The repair of long-segment tracheal defects remains a challenge in clinical practice. Conventional end-to-end anastomosis is not suitable for the treatment of long-segment defects because excessive tension at both ends may result in anastomotic fistula. Thus, appropriate substitutes for tracheal replacement are urgently needed to meet clinical demand. A solid prosthesis was previously investigated as a potential substitute; however, the short- and long-term prognoses of patients who received this prosthesis were unsatisfactory because of complications such as infection and anastomotic fistula.[20–22] Allograft tracheal transplantation has also been used to treat long-segment defects; however, it has limitations, such as lifelong demand for immunosuppressive therapy, challenges in revascularization, and complex surgical procedures, which can ultimately result in necrosis and even tracheomalacia.[3,23]

Tissue engineering makes it possible for researchers to collect autologous cells and biofabricate tissues or even organs to meet clinical demands. In tissue engineering approaches, seeding cells, scaffolds, and growth factors are combined to generate a structure that can function like native tissues or organs.[24] For tracheal tissue engineering, researchers have fabricated various products to reconstruct long-segment defects. Decellularized tracheal matrix seeding with autologous cells has been the main approach for long-segment tracheal reconstruction. In this approach, cells are removed from an allogeneic or xenogeneic trachea, as they can trigger an immune response, and nearly all of the ECM is preserved without significant impacts on mechanical strength. Seeding cells provide regenerative properties so that implants can generate new matrices to replace decellularized matrices.[8,9]

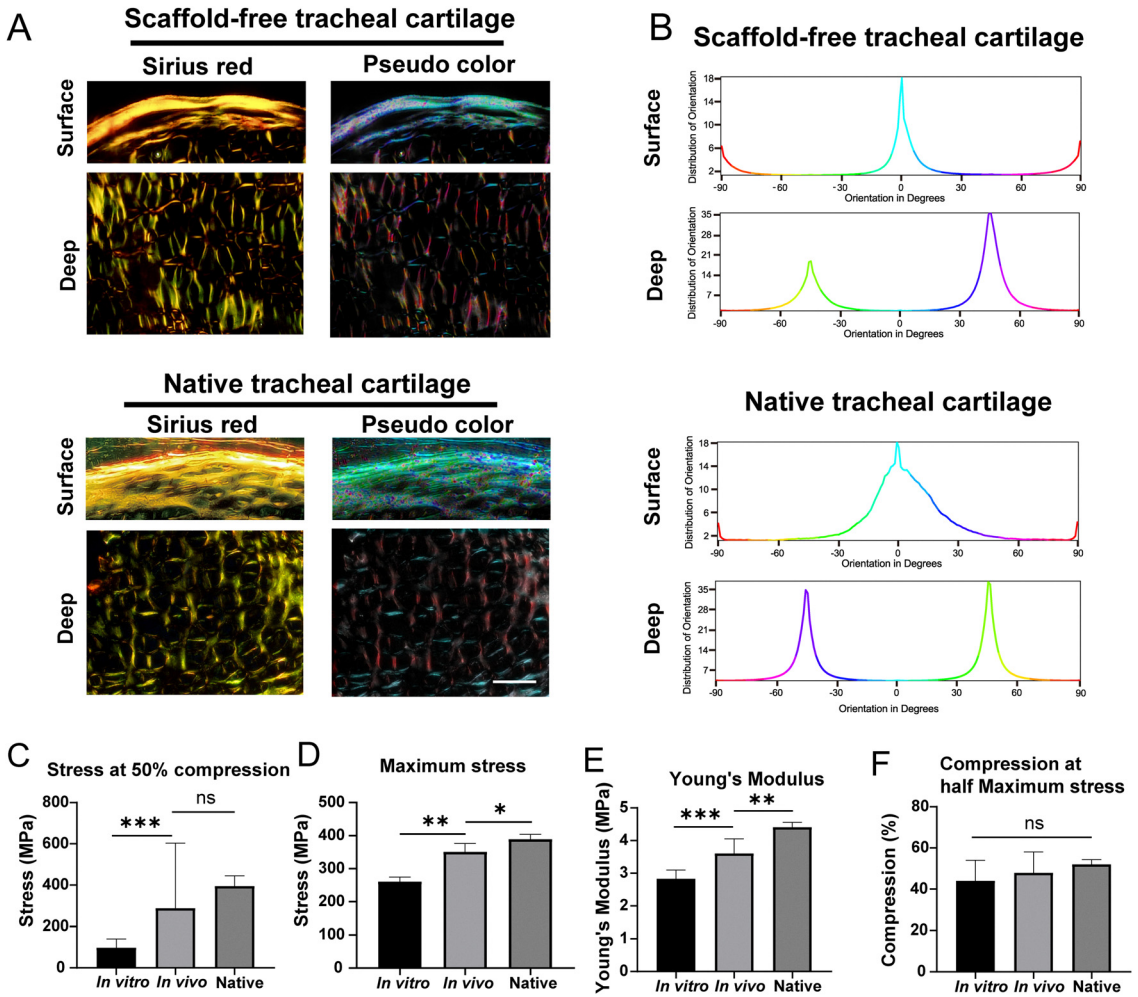

Fig. 6 Fibrous arrangement and mechanical strength of the scaffold-free tracheas. (A) Images and pseudocolor image of Sirius Red staining of scaffold-free tracheal cartilage and native tracheal cartilage. (B) Quantification of the collagen fiber orientations in the superficial zone and deep zone of scaffold-free tracheal cartilage and native tracheal cartilage. Compressive modulus values (C), stress at 50% compression (D), Young's modulus (E), and compression at half maximum stress (F) for the scaffold-free tracheal wall and lumen *in vitro* and *in vivo*, compared to that of the native trachea. Scalebar: 50 μm.

Polycaprolactone (PCL) is the most commonly used biodegradable material, and it has both good biocompatibility and mechanical strength.[7] With the help of these scaffolds, tissue engineering of the trachea has the potential to overcome the difficulties associated with the treatment of long-segment tracheal defects.

Scaffold-free technology is another branch of tissue engineering. As scaffold-free tissue engineering does not use polymers as a main component, it has the highest cell density.[16] Scaffold-free technology has been widely applied to biofabricate tubular structures, such as blood vessels, corneas, and skin.[15,16,25] As scaffold-free tissue engineering uses autologous cells, no immune response is triggered, which means that no immunosuppressive agents need to be administered after surgery. Because no scaffold material is used, no biodegradation occurs, resulting in stable mechanical strength of the grafts after surgery. Cells are inclined to aggregate as a microtissue. This bottom-up approach relies on self-assembly or the directed assembly of cells. As a result of the 3D structure of cell aggregates, cell–cell interactions are enhanced, and aggregates exhibit various properties, such as increased viability, increased matrix production, and improved cell function. For example, pancreatic cell aggregates have insulin, glucagon, and somatostatin excretion abilities.[26] Chondrocyte aggregates have been shown to express higher levels of collagen II and aggrecan.[27] As a result, cell aggregates may be used as building blocks for scaffold-free tissue engineering. Considering this context, we designed a scaffold-free tissue engineering approach to biofabricate tubular tracheal substitutes and studied the biocompatibility and mechanical strength of the grafts *in vitro* and *in vivo* to provide a novel solution for treating long-segment tracheal defects.

In this work, spheroids were automatically aggregated with the help of agarose molds fabricated with homemade molds. Many techniques have been developed to generate cell aggregates thus far. Initially, cells were aggregated in culture dishes

with nonadhesive surfaces or *via* spinner culture.[28,29] These methods produce spheroids with a highly variable diameter, hindering their application. Then, a hanging drop method was invented.[30] However, even with the help of high-throughput screening instruments, the hanging drop technique is still not efficient enough to produce spheroids for use as building blocks in tissue engineering.[31] Fusion of spheroids into a continuous structure was observed macroscopically; future work should quantify fusion efficiency and integration quality. With the help of agarose molds, chondrocytes aggregated as spheroidal microtissues. The diameters of the spheroids varied with the initial cell density seeded on day 0. Thus, we could control the diameters of the cartilage spheroids by seeding a specific number of cells, as shown by the function $d = 15.020\sqrt[3]{x} - 19.572$. Then, we further studied the factors that influenced the spheroid diameter. After long-term incubation, we found that the diameter showed a trend of first decreasing and then increasing over time. Combining that finding with the outcomes of subsequent histology experiments, we divided the growth conditions of the spheroids into three stages. In the first stage, from day 0 to day 3, the cells in the spheroids aggregated, resulting in a decreased diameter of the spheroids. In the second stage, from day 4 to day 14, the intercellular space grew, showing that ECM was actively accumulated and cartilage lacunae formed, resulting in an increased diameter of the spheroids. In the third stage, from day 15, the cartilage spheroids became mature, with a stable diameter, ECM accumulation and more distinct lacunae.

Chondrocytes in spheroids secreted more ECM than those cultured in dishes. As shown previously, spheroids have plenty of useful properties, such as regenerative ability, matrix production, and differentiation properties. Chondrocyte spheroids have similar properties, as previously reported.[27] On the one hand, intercellular contact and communication promote matrix production; on the other hand, the ECM plays an important role in cell proliferation, differentiation, and maintenance of homeostasis.[32] In this study, we performed a spreading test and live/dead staining of the spheroids, demonstrating that the chondrocyte spheroids had good regenerative potential. However, cartilage-related gene expression was compared between cells in spheroids and those on dishes. The results showed that genes related to cartilage regeneration, such as GAG and SOX9, were expressed at significantly higher levels in spheroids than in dishes. The constructs display early hyaline cartilage-like features, but further validation is required to confirm tissue maturity and specificity. Subsequent histological staining confirmed cartilaginous matrix accumulation around the cells.

We further optimized the spheroid culture conditions to stimulate maximal matrix accumulation. First, the cell number was optimized. Spheroids aggregated from 2k cells showed the greatest migration among spheroids of different sizes, as shown in Fig. 2H and described previously. Furthermore, as the cell number increased, the relative expression of every related gene first increased and then decreased. Spheroids aggregated from 2k cells relatively expressed higher COL2A1, GAG, and SOX9 in different groups. These results indicated that 2k cells per spheroid was the most appropriate number to promote matrix production. The constructs demonstrated cartilage matrix deposition within 4 weeks, suggesting a relatively fast tissue formation timeline under these conditions. Thus, we chose 2k cells as the optimal cell number to generate spheroids for further study. Then, we cultured the spheroids in different media. PCR results showed that compared to expansion medium, ITS medium stimulated COL2A1 expression, although the difference was not statistically significant. In addition, differentiation medium stimulated COL2A1 and GAG, and the difference was statistically significant, indicating that differentiation medium was more appropriate for culturing the spheroids. In summary, spheroids formed from 2k cells, cultured in differentiation medium for 2 days, were most appropriate for use as ''building blocks'' for scaffold-free tissue engineering.

Chondrocyte spheroids were able to fuse and form doublets, as shown above. This fusion process of chondrocyte spheroids was different from that of tumor spheroids, which ultimately formed larger spheroids.[33] However, the fusion process was triggered by contact between spheroids, as shown above, similar to other spheroidal fusion processes. Our results showed that, 2 days after placing the spheroids together in the microwell, they came into contact and began to fuse. The fusion process was completed within 3 days. The tissue within the doublets was continuous, with initial cell connection and subsequent matrix accumulation. When the spheroids were placed on a nonadhesive surface, they fused completely, with a reduction in size.[12] To prevent the spheroids from shrinking, we cast agarose molds to maintain the initial shape of the scaffold-free tracheas during the self-assembly process. The results showed that the spheroids maintained a tubular structure and fused into a scaffold-free trachea.

To date, only a few studies have focused on constructing tissue-engineered scaffold-free tracheas. Mark and colleagues fabricated scaffold-free cartilage sheets to repair 20 mm tracheal defects with the help of silicone tubes and muscle flaps, which were proven to have adequate stability.[6] Interestingly, Dikina *et al.*[34,35] provided an excellent perspective on fabricating complex tracheal structures. They employed human mesenchymal stem cells (hMSCs) to form ring-shaped constructs within molds and then assembled multiple rings into tubular structures with favorable mechanical properties. In our study, the tubular building blocks were generated through careful optimization, identifying 2000 cells per microwell as the most suitable seeding density. Then, we deposited prefunctionalized chondrocyte microtissues for self-assembly into scaffold-free tracheas. The scaffold-free tracheas were supported by a 1% agarose mold that had a low-adhesion surface to prevent adhesion and was strong enough to prevent excessive wall thickening. Daily observation showed that self-assembly was completed within 3 days; subsequent histological results revealed that the spheroids had self-assembled into a complete tubular structure, and traces of spheroids were observed. In our study, the tubular structure exhibited abundant Safranin O and Alcian Blue staining, indicating frequent cell interactions and consecutive matrix production. Based on *in vivo* examination of

scaffold-free tracheas, we concluded that the *in vivo* process was necessary. First, chondrocytes in the scaffold-free tracheas were viable, providing regenerative ability to the cartilage. This is important because the matrix is renewable *in vivo* and chondrocytes are needed. Second, an abundant matrix accumulated, giving the trachea sustained and appropriate mechanical strength. Third, the scaffold-free trachea was wrapped by surrounding tissues, with a blood supply. These results proved that the scaffold-free trachea was biocompatible, and the blood vessels supplied nutrition and oxygen. Finally, the tissue-engineered trachea requires a balance of flexibility to accommodate neck movement and stiffness to resist collapse under negative airway pressure. The modulus of compression and modulus of elasticity need to be close to that of the native trachea. Therefore, the testing of these mechanical properties also needs to be considered further in future research.[19]

Our study has many advantages. First, no polymers were used for tissue engineering of the scaffold-free tracheas, avoiding inflammation and subsequent collapse caused by polymer degradation. Second, the scaffold-free tracheas had abundant chondrocytes and matrix, which resulted in good regenerative ability, with high cell viability, increased proliferative activity, and dynamic morphological development. Third, host-derived vascularization was observed in the constructs, which may contribute to tissue survival and maturation.

Although the scaffold-free tracheas were proven to be biologically regenerative and mechanically strong, there remain some limitations. First, this study lacks functional assessments under physiological conditions, such as dynamic mechanical testing, airflow resistance evaluation, mucosal regeneration, and long-term durability. Future studies will assess physiological performance in animal models. Second, in our study, there is an absence of quantitative assays due to limited laboratory resources at the time of experimentation. Future work will integrate these standardized methods to provide a more rigorous assessment of tissue quality. Third, the relatively short 4-week subcutaneous implantation precludes assessment of long-term viability, durability, tissue remodeling, and immune response. Future studies will extend implantation to 12 weeks or more and evaluate parameters such as cartilage hypertrophy, degradation, calcification, dimensional stability, and immune infiltration. Finally, further investigation of the orthotopic implantation and clinical application of the biofabricated tracheas for long-term use is still needed.

4. Conclusion

In summary, it was feasible to promote the self-assembly of spheroids that were aggregated from chondrocytes and cultured under optimized conditions into scaffold-free tracheas by depositing them in agarose molds. The tissue-engineered scaffold-free trachea was proven to have satisfactory regenerative ability and mechanical strength; however, further investigation should be conducted to verify its performance after orthotopic implantation.

5. Experimental section

Isolation and culture of primary chondrocytes

Chondrocytes were harvested from auricular cartilage of New Zealand white rabbits. Tissue was minced and digested sequentially with pepsin (0.25 mg mL^{-1}, 1 h) and type II collagenase (0.2%, 6 h) at 37 °C. Released chondrocytes were filtered, centrifuged, and cultured in expansion medium (EM). Cells were expanded to passage 3 (P3) before spheroid formation. EM was made from Dulbecco's modified Eagle medium (DMEM) containing 10% fetal bovine serum (FBS) and 1% penicillin–streptomycin (PS).

Formation of chondrocyte spheroids

An agarose mold was prepared with a homemade template to support the formation of microwells on the agarose gel surface (Fig. S1A–D). Briefly, a boiled solution of 1% agarose (2 mL) in phosphate-buffered saline (PBS) buffer was added to a 6-well plate. The template was immediately placed into the solution and carefully removed to allow complete solidification of the agarose solution. After 30 min of exposure to UV light, the agarose mold was rinsed with PBS. The chondrocytes were seeded into the agarose mold at cell densities of 1–16k per microwell in chondrogenic DM. The DM was made with 96% DMEM, 1% proline, 1% ascorbic acid, 1% penicillin–streptomycin (PS) and 1% ITS. The ITS medium was made with 98% DMEM, 1% PS and 1% ITS.

Cell viability assessment

Cell viability was investigated with a live/dead assay kit (Molecular Probes, Invitrogen, USA). Fluorescent agent dye was added after washing, and the cells were viewed with a fluorescence microscope (IX75, Olympus, Japan) at wavelengths of 495 and 515 nm.

Fusion process

Two spheroids were placed into the same microwell. As the two spheroids approached each other, the doublet length, doublet width, intersphere angle and contact length were recorded daily.

Scaffold-free trachea mold

Tubular agarose molds were fabricated with homemade templates. After being stamped with a tubular template, the 1% and 0.3% (wt) agarose formed an empty vacant position of tubular shape. Each mold had an outer diameter of approximately 7.5 mm, an inner diameter of approximately 5.0 mm, and a wall thickness of approximately 1.2 mm. Spheroids were seeded into the tubular space after the molds were exposed to UV light for 30 min and rinsed with PBS. The scaffold-free tracheas were ultimately cultured in chondrocyte differentiation medium. The wall thickness of the tracheas was measured at the top, left, bottom, and right positions every day. After 28 days of culture, the tubular molds were removed, and the scaffold-free tracheas were fabricated.

Implantation

A total of 18 six-week-old BALB/c nude mice were used for subcutaneous implantation. Constructs were implanted under general anesthesia with 4% chloral hydrate (10 mL kg^{-1}, intraperitoneally). Each pre-assembled cartilage tube was placed subcutaneously and maintained for 4 weeks, after which constructs were harvested for histological, biochemical, and molecular analyses. All procedures were performed in accordance with institutional guidelines and approved by the Shanghai Pulmonary Hospital Ethics Committee (K22-158Y). Endpoints were defined as the 4-week retrieval time, and all procedures were performed consistently across animals.

Gene expression

Cells or tissues were immersed in 1 mL of TRIzol reagent for 5 min to extract RNA. 0.2 mL of chloroform was added and mixed vigorously. The mixture was incubated at room temperature for 15 min and centrifuged for 15 min at 12 000 rpm. The upper aqueous layer was collected, and the same volume of isopropanol was added; the mixture was centrifuged for 10 min at 12 000 rpm after 10 min of incubation. The sediment was washed with 1 mL of 75% ethanol and centrifuged for 5 min at 12 000 rpm. The sediment was resuspended in 50 μL of diethylpyrocarbonate (DEPC) water for storage. The extracted RNA was then reverse-transcribed to cDNA and used for a quantitative real-time polymerase chain reaction (q-PCR). The following rabbit primers were used: (1) COL1A1 (forward primer: 5′-GGC AAC AGC AGG TTC ACT TAC-3′, reverse primer: 5′-GGC AAA CGA GAT GGC TTA T-3′); (2) COL2A1 (forward primer: 5′-CCT TGG TGG AAA CTT TGC TGC-3′, reverse primer: 5′-GGG TTG CCT TGA AAT CCT TGC-3′); (3) GAG (forward primer: 5′-AGG TCG TGG TGA AAG GTG TTG-3′, reverse primer: 5′-GTA GGT TCT CAC GCC AGG GA-3′); (4) SOX9 (forward primer: 5′-GTA CCC GCA CCT GCA CAA C-3′, reverse primer: 5′-TCC GCC TCC TCC ACG AAG-3′); (5) GAPDH (forward primer: 5′-GGA GAA AGC TGC TAA-3′, reverse primer: 5′-ACG ACC TGG TCC TCG GTG TA-3′).

Histological analysis

Dehydration process: the sample was fixed in 4% paraformaldehyde solution overnight, embedded in paraffin, and then cut into 6 μm sections for staining. H&E staining: sections were routinely rehydrated with distilled water. The sections were immersed in hematoxylin for 5 min, and then washed in tap water for approximately 5 min until the sections turned blue. The sections were kept in 75% ethanol containing 1% HCl for 3 seconds and then flushed with tap water until the sections turned blue again. The sections were stained with eosin for 1 minute. The sections were routinely dehydrated with dimethylbenzene and then mounted on coverslips with neutral balsam. Alcian Blue/Nuclear Fast Red (A&N) staining: sections were routinely rehydrated in distilled water and then immersed in Alcian Blue solution for 30 min. After sufficient washing in tap water, Nuclear Fast Red staining was performed for 10 min. The sections were rinsed with 100% ethanol 3 times. Then, the sections were dehydrated twice with dimethylbenzene and mounted on coverslips with neutral balsam. Safranin O/Fast Green (S&F) staining: sections were routinely rehydrated in distilled water and then immersed in Fast Green solution for 5 min. The slides were flushed with tap water and then stained with Safranin O for 10 seconds. The sections were washed with 100% ethanol 3 times and then dehydrated in dimethylbenzene twice. The coverslips were mounted using neutral balsam. SR staining: sections were routinely rehydrated with distilled water. SR was dropped onto the sections for 20 min. Then, the dye was rinsed with flowing water. Mayer's hematoxylin was added to stain the nucleus for 8 to 10 min. The dye was removed by flushing with water for 10 min. Then, the sections were routinely dehydrated twice with dimethylbenzene and mounted on coverslips with neutral balsam. Collagen II and CD31 IHC: sections were stained with primary antibodies against collagen II (1 : 200, ab34712) or CD31 (1 : 500, ab222783), followed by a horseradish-peroxidase-conjugated anti-rabbit antibody. Color development was then performed with diaminobenzidine tetrahydrochloride (Santa Cruz).

Mechanical analysis

The load-bearing ability of the tracheas was tested *via* a compressive moduli test with tracheal walls. Mechanical testing was performed on $n = 3$ constructs per group using a universal mechanical tester (5542, Instron). All specimens were tested in a hydrated state after immersion in PBS at room temperature for 30 min to allow equilibration. Compression was applied at a displacement-controlled rate of 1 mm min^{-1} until 50% strain. Stress–strain curves were obtained, and parameters including stress at 50% strain, maximum stress, Young's modulus, and compression at half maximum stress were calculated.

Statistical analysis

All continuous data are presented as the mean and standard deviation (SD), and categorical data are presented as numbers. A Student's *t*-test was performed to compare continuous variables between two groups. One-way ANOVA was performed for comparisons of continuous variables among more than two groups, and a *post hoc* test was performed when one-way ANOVA indicated a significant difference, followed by a Tukey's *post hoc* multiple comparison test when parametric assumptions were satisfied. When assumptions were not met, the Kruskal–Wallis test was applied as a nonparametric alternative. Linear regression was performed to evaluate the relationship between the cell density and the diameter of the spheroids. Statistical significance was defined as $p < 0.05$. All analyses were performed using GraphPad Prism 9.0 (GraphPad Software, USA).

Author contributions

Long Wang: investigation, methodology, formal analysis, writing – original draft. Weikang Lin: methodology, formal analysis of animal experiments. Lei Zhang: methodology, formal analysis of immunochemical analysis. Yunlang She:

methodology, formal analysis of biochemical analysis. Weiyan Sun: methodology, formal analysis of microsphere characteristics. Hai Tang: resources, formal analysis. Chao Lin: conceptualization, formal analysis, resources, review & editing, funding acquisition. Chang Chen: conceptualization, formal analysis, writing original draft, review & editing, funding acquisition. All authors proofread the manuscript and agreed on the final version.

Conflicts of interest

The authors declare that they have no known competing financial interests or personal relationships that could have appeared to influence the work reported in this paper.

Abbreviations

ECM	Extracellular matrix
EM	Expansion medium
DM	Differentiation medium
ITS	Insulin–transferrin–selenium
H&E	Hematoxylin and eosin
A&N	Alcian Blue/Nuclear Fast Red staining
S&F	Safranin O/Fast Green staining
SR	Sirius Red staining
IHC	Immunohistochemistry
PCL	Polycaprolactone
DMEM	Dulbecco's Modified Eagle Medium
FBS	Fetal bovine serum
PS	Penicillin–streptomycin
PBS	Phosphate-buffered saline
DEPC	Diethylpyrocarbonate
qPCR	Quantitative real-time polymerase chain reaction

Data availability

The datasets used and/or analyzed during the current study are available from the corresponding author on reasonable request.

Supplementary information (SI): Fig. S1 Process of spheroid construction. (A) 3D view of the in-house made spheroid template at different angles. Gross appearance of the in-house made spheroid template (B) and molding in a six-well plate (C). (D) Gross appearance of an agarose spheroid mold in a six-well plate. Chondrocytes were seeded into microwells on day 0 (E), and chondrocyte spheroids formed on day 15 (F). (G) and (H) Macroscopic images of spheroid in a single well of a six-well plate. (I) Daily microscopy of spheroid in a microwell. (J) The diameters of spheroids formed with different chondrocyte numbers per microwell. Linear regression of spheroid diameter *vs.* chondrocyte numbers per microwell. (K) Normal distribution of spheroid diameter with different chondrocyte numbers per microwell. Fig. S2 3D view of the scaffold-free tracheal mold at different angles. (A) Gross view. (B) Front view. (C) Lateral view. (D) Top view. Fig. S3 Characteristics of the scaffold-free tracheas. (A) Microscopic morphology changes in the scaffold-free tracheal wall after different culture times. The thickness of the tracheal wall for scaffold-free tracheas fabricated in 1% (B) and 0.3% (C) agarose molds for different culture times and on different sides. Scalebar: 200 μm. See DOI: **https://doi.org/10.1039/d5ma00172b**.

Acknowledgements

This research was sponsored by Noncommunicable Chronic Diseases-National Science and Technology Major Project (2024ZD0529000), Shanghai Pulmonary Hospital Innovation Team (No. fkcx2306), Clinical Research Foundation of Shanghai Pulmonary Hospital, (No. SKPY2021005), the Science and Technology Commission of Shanghai Municipality (No. 21YF1438500), Science and Technology Commission of Shanghai Municipality (No. 21S31905200). This study was approved by the Shanghai Pulmonary Hospital Ethics Committee.

References

1 M. Den Hondt and J. J. Vranckx, Reconstruction of defects of the trachea, *J. Mater. Sci.: Mater. Med.*, 2017, **28**(2), 24.
2 C. D. Wright, B. B. Graham, H. C. Grillo, J. C. Wain and D. J. Mathisen, Pediatric tracheal surgery, *Ann. Thorac. Surg.*, 2002, **74**(2), 308–313.
3 H. C. Grillo, Tracheal replacement: a critical review, *Ann. Thorac. Surg.*, 2002, **73**(6), 1995–2004.
4 P. Delaere, D. Van Raemdonck and J. Vranckx, Tracheal transplantation, *Intensive Care Med.*, 2019, **45**(3), 391–393.
5 L. Soriano, T. Khalid and D. Whelan, *et al.*, Development and clinical translation of tubular constructs for tracheal tissue engineering: a review, *Eur. Respir. Rev.*, 2021, **30**(162), 210154.
6 M. Weidenbecher, H. M. Tucker, D. A. Gilpin and J. E. Dennis, Tissue-engineered trachea for airway reconstruction, *Laryngoscope*, 2009, **119**(11), 2118–2123.
7 M. Gao, H. Zhang and W. Dong, *et al.*, Tissue-engineered trachea from a 3D-printed scaffold enhances whole-segment tracheal repair, *Sci. Rep.*, 2017, **7**(1), 5246.
8 Y. Xu, D. Li and Z. Yin, *et al.*, Tissue-engineered trachea regeneration using decellularized trachea matrix treated with laser micropore technique, *Acta Biomater.*, 2017, **58**, 113–121.
9 C. R. Butler, R. E. Hynds and C. Crowley, *et al.*, Vacuum-assisted decellularization: an accelerated protocol to generate tissue-engineered human tracheal scaffolds, *Biomaterials*, 2017, **124**, 95–105.
10 M. A. Gionet-Gonzales and J. K. Leach, Engineering principles for guiding spheroid function in the regeneration of bone, cartilage, and skin, *Biomed. Mater.*, 2018, **13**(3), 034109.
11 S. Lopa, F. Piraino and R. J. Kemp, *et al.*, Fabrication of multi-well chips for spheroid cultures and implantable constructs through rapid prototyping techniques, *Biotechnol. Bioeng.*, 2015, **112**(7), 1457–1471.

12 V. Beachley, V. Kasyanov and A. Nagy-Mehesz, *et al.*, The fusion of tissue spheroids attached to pre-stretched electrospun polyurethane scaffolds, *J. Tissue Eng.*, 2014, **5**, 2041731414556561.
13 J. M. Kelm, V. Lorber and J. G. Snedeker, *et al.*, A novel concept for scaffold-free vessel tissue engineering: self-assembly of microtissue building blocks, *J. Biotechnol.*, 2010, **148**(1), 46–55.
14 A. P. Napolitano, D. M. Dean and A. J. Man, *et al.*, Scaffold-free three-dimensional cell culture utilizing micromolded nonadhesive hydrogels, *Biotechniques*, 2007, **43**(4), 496–500.
15 F. N. Syed-Picard, Y. Du and A. J. Hertsenberg, *et al.*, Scaffold-free tissue engineering of functional corneal stromal tissue, *J. Tissue Eng. Regener. Med.*, 2018, **12**(1), 59–69.
16 C. Norotte, F. S. Marga, L. E. Niklason and G. Forgacs, Scaffold-free vascular tissue engineering using bioprinting, *Biomaterials*, 2009, **30**(30), 5910–5917.
17 X. Wang, Z. Li and T. Shi, *et al.*, Injectable dextran hydrogels fabricated by metal-free click chemistry for cartilage tissue engineering, *Mater. Sci. Eng., C*, 2017, **73**, 21–30.
18 J. Ahn, D. H. Kim and D. J. Koo, *et al.*, 3D microengineered vascularized tumor spheroids for drug delivery and efficacy testing, *Acta Biomater.*, 2023, **165**(1878–7568), 153–167.
19 J. M. Zuidema, M. M. Pap, D. B. Jaroch, F. A. Morrison and R. J. Gilbert, Fabrication and characterization of tunable polysaccharide hydrogel blends for neural repair, *Acta Biomater.*, 2011, **7**(4), 1634–1643.
20 W. E. Neville, J. P. Bolanowski and G. G. Kotia, Clinical experience with the silicone tracheal prosthesis, *J. Thorac. Cardiovasc. Surg.*, 1990, **99**(4), 604–612.
21 H. Toomes, G. Mickisch and I. Vogt-Moykopf, Experiences with prosthetic reconstruction of the trachea and bifurcation, *Thorax*, 1985, **40**(1), 32–37.
22 C. Debry, N. E. Vrana and A. Dupret-Bories, Implantation of an Artificial Larynx after Total Laryngectomy, *N. Engl. J. Med.*, 2017, **376**(1), 97–98.
23 P. Delaere, J. Vranckx, G. Verleden, P. De Leyn and D. Van Raemdonck, Tracheal allotransplantation after withdrawal of immunosuppressive therapy, *N. Engl. J. Med.*, 2010, **362**(2), 138–145.
24 A. J. Boys, S. L. Barron, D. Tilev and R. M. Owens, Building Scaffolds for Tubular Tissue Engineering, *Front. Bioeng. Biotechnol.*, 2020, **8**, 589960.
25 F. Kawecki, D. Mayrand and A. Ayoub, *et al.*, Biofabrication and preclinical evaluation of a large-sized human self-assembled skin substitute, *Biomed. Mater.*, 2021, **16**(2), 025023.
26 Y. H. Jo, I. J. Jang and J. G. Nemeno, *et al.*, Artificial islets from hybrid spheroids of three pancreatic cell lines, *Transplant. Proc.*, 2014, **46**(4), 1156–1160.
27 Y. Shi, J. Ma, X. Zhang, H. Li, L. Jiang and J. Qin, Hypoxia combined with spheroid culture improves cartilage specific function in chondrocytes, *Integr. Biol.*, 2015, **7**(3), 289–297.
28 J. E. Frith, B. Thomson and P. G. Genever, Dynamic three-dimensional culture methods enhance mesenchymal stem cell properties and increase therapeutic potential, *Tissue Eng., Part C*, 2010, **16**(4), 735–749.
29 J. Friedrich, C. Seidel, R. Ebner and L. A. Kunz-Schughart, Spheroid-based drug screen: considerations and practical approach, *Nat. Protoc.*, 2009, **4**(3), 309–324.
30 I. Martinez, J. Elvenes, R. Olsen, K. Bertheussen and O. Johansen, Redifferentiation of in vitro expanded adult articular chondrocytes by combining the hanging-drop cultivation method with hypoxic environment, *Cell Transplant.*, 2008, **17**(8), 987–996.
31 Y. C. Tung, A. Y. Hsiao, S. G. Allen, Y. S. Torisawa, M. Ho and S. Takayama, High-throughput 3D spheroid culture and drug testing using a 384 hanging drop array, *Analyst*, 2011, **136**(3), 473–478.
32 M. A. Kinney, T. A. Hookway, Y. Wang and T. C. McDevitt, Engineering three-dimensional stem cell morphogenesis for the development of tissue models and scalable regenerative therapeutics, *Ann. Biomed. Eng.*, 2014, **42**(2), 352–367.
33 N. V. Kosheleva, Y. M. Efremov and B. S. Shavkuta, *et al.*, Cell spheroid fusion: beyond liquid drops model, *Sci. Rep.*, 2020, **10**(1), 12614.
34 A. D. Dikina, H. A. Strobel, B. P. Lai, M. W. Rolle and E. Alsberg, Engineered cartilaginous tubes for tracheal tissue replacement via self-assembly and fusion of human mesenchymal stem cell constructs, *Biomaterials*, 2015, **52**, 452–462.
35 A. D. Dikina, D. S. Alt, S. Herberg, A. McMillan, H. A. Strobel, Z. Zheng, M. Cao, B. P. Lai, O. Jeon, V. I. Petsinger, C. U. Cotton, M. W. Rolle and E. Alsberg, A Modular Strategy to Engineer Complex Tissues and Organs, *Adv. Sci.*, 2018, **5**(5), 1700402.